Electronic Supplementary Material (ESI) for Inorganic Chemistry Frontiers.

A synergistic {Cu_2-$W_{12}O_{40}$} catalyst with high conversion for homo-coupling of terminal alkynes

Zhan-Guo Jiang,[#] Hui-Min Zeng,[#] Xiangyu Zhang, Yuan Tan, You-Zhao Lan, Yu Wang, De-Liang Long,* Leroy Cronin* and Cai-Hong Zhan*

Table of Contents

S1. Materials

All starting materials and reagents were purchased from commercial suppliers and used without further purification. Na_2WO_4 and $Cu(CH_3COO)_2\cdot2H_2O$ (AR) were purchased from Aladdin. CH_3COOH (AR) as well as concentrated hydrochloric acid (AR) were purchased from Sinopharm Chemical Reagent Co., Ltd., China.

S2. General Experimental Section

Powder X-ray Diffraction (PXRD)

Powder XRD patterns were obtained using a Bruker D8 Advance X-ray diffractometer with (λ (CuKα) = 1.5405 Å) radiation.

Fourier Transform Infrared Spectroscopy (FTIR)

The materials were recorded on KBr disk using a Nicolet NEXUS 670 spectrometer between 400 and 4000 cm^{-1}.

Thermogravimetric Analyses (TGA)

They were carried out on a TA Instruments STA499 F5 thermobalance with a 100 $mL\cdot min^{-1}$ flow of nitrogen; the temperature was ramped from 20°C to 800°C at a rate of $5°C\cdot min^{-1}$.

Elemental Analyses (EA)

C H microanalyse was performed on a Perkin-Elmer 240C elemental analyser.

Cyclic voltammetry (CV)

Cyclic voltammetry (CV) experiments were performed in water at room temperature using a VersaSTAT 3F instrument (Advanced Measurement Technology Inc.). All CV experiments were performed using a glass carbon (GC) electrode with a diameter of 3 mm as the working electrode. Before use, the electrode surface should be regularly polished with 0.05 μm aluminum oxide slurry on the felt surface. The counter electrode is a Pt wire, and the reference electrode is a saturated calomel electrode (SCE) electrode. After dissolving **1** in water, the scan rate at 0.1 M at 298 K is 0.05V s^{-1}.

X-ray photoelectron spectroscopy (XPS)

An ESCALAB 250Xi (Thermo Fisher Scientific) was used for X-ray photoelectron spectroscopy (XPS) analysis, and monochromatic AlKα (1486.6eV) was used as the excitation source. After complete removal of the moisture in the catalysts (It should be notable that the observation of dark blue solution is transitory in the first step in Scheme 2 and immediately, the catalyst is collected by addition of an excess of diethyl ether (precipitation method) to do the XPS) by drying at 100 °C for 24h, the catalysts were analyzed without surface sputtering and etching, so that the degree of vacuum in the XPS equipment was maintained at (10–6) Pa. Spectra were analyzed using XPS PEAK software (version 4.1). The intensities were estimated from the integration of each peak, subtraction of the Shirley background, and fitting of the experimental curve to a combination of Lorentzian and Gaussian lines of various proportions. All binding energies were referenced to the C1s line at 284.8eV. Binding energy values were measured with a precision of ±0.3eV.

Coupling reaction catalysis

GC/MS experiments were performed using an Agilent Technologies 7890B GC System interfaced with a 5977B EI mass spectrometer. Dichloromethane was used as a solvent and the sample was injected in 2 µL portions onto a HP5-MS column (30 m X 0.25 mm X 0.25 µm). The operating method was programmed with a 3.00 min solvent delay. The initial temperature was set at 80 °C and held for 2 min. The temperature was ramped at 20 °C per min to 250 °C and was held for 6.00 min. In a typical reaction, a mixture of phenylacetylene (1 mmol), **1** (0.1g, 3 mol%) was stirred in an atmosphere at room temperature in DMF (3 mL). The reaction progress was monitored by gas chromatography.

In situ DRIFTS of homo-coupling of phenylacetylene

The in-situ DRIFTS (Diffuse Reflectance Infrared Fourier Transform Spectroscopy) of phenylacetylene were recorded on the instrument of Bruker INVENIO Fourier transform infrared spectrometer equipped with a MCT detector in the range 600–4000 cm^{-1}. Before the test, the catalyst was packed into a sample cell with one KBr window and two ZnSe windows.

With the protection of helium, 10 μL of DMF was introduced into the sample and the background spectrum was recorded. Afterwards, 10 μL of phenylacetylene was introduced into the sample for adsorption. Subsequently, the reaction temperature was increased to a fixed temperature with a heating rate of 5 °C/min. After approaching to steady state (about 10 min), the spectra were collected at 40, 60, 80, and 100 °C, respectively.

Single-crystal X-ray diffraction (SCXRD)

A suitable crystal of **1** was mounted in a Hampton cryoloop with Paratone® N oil cryoprotectant. Intensity data collections were carried out at T =150(2) K with a Bruker D8 VENTURE diffractometer equipped with a PHOTON 100 CMOS bidimensional detector using a high brilliance IμS microfocus X-ray Mo Ka monochromatized radiation (λ = 0.71073 Å). The structures were solved by intrinsic phasing methods and refined by full-matrix least squares using the SHELX-TL package.[1] All atoms were refined with anisotropic thermal parameters except for solvent molecules. Hydrogen atoms on water and POM are not identified. Positions of the remaining hydrogen atoms were calculated and refined isotropically using the gliding mode. Further details about of the crystal structure determinations may be obtained free of charge via the Internet at https://www.ccdc.cam.ac.uk/. CCDC 2151867. Crystallographic data for single-crystal X-ray diffraction studies are summarized in Table S1.

S3. Synthesis and Experimental Section

Synthesis of 1

$Na_6(H_2W_{12}O_{40})[Cu_4(CH_3COO)_8]\cdot 15H_2O$

$Na_2WO_4\cdot 2H_2O$ (5.02 g, 15.2 mmol) and $Cu(CH_3COO)_2\cdot H_2O$ (0.79 g, 4 mmol) were first dissolved in water (15 ml and 10 ml, respectively) at 80 ˚C, and the above $Cu(CH_3COO)_2$ solution then added into Na_2WO_4 solution drop by drop, after that the pH of this mixture was adjusted to 3.24 by addition of acetic acid. The whole operation was at 80 ˚C. The solution was kept at 80 ˚C under stirring for 100 minutes, and then the pH was adjusted to 2.57 by addition of 70% nitric acid. Finally, the solution was cooled, filtered and left to evaporate slowly. Green plate shaped crystals appeared after three days. Yield: 0.32 g. Elemental analysis, calc. for $C_{16}H_{56}O_{71}Na_6Cu_4W_{12}$: Elemental analysis: Calc. (found): H 1.5 (1.4); C 4.8 (4.8); W 48.9 (49.62); Cu 6.1 (5.65); Na 1.3 (1.27).

S4 Crystal data and structure refinement

Table S1. Crystal data and structure refinement for **1**.

Chemical formula	$C_{16}H_{24}Cu_4Na_6O_{64}W_{12}$
Formula weight	3838.52 g/mol
Temperature	150(2) K
Wavelength	0.71073 Å
Crystal size	0.1 × 0.1 × 0.1 mm
Crystal system	tetragonal
Space group	$I\bar{4}m2$
Unit cell dimensions	a = 17.28 Å, b = 17.28 Å, c = 13.05 Å
	α = 90° β = 90° γ = 90°
Volume	3903.4(5) $Å^3$
Z	2
Density (calculated)	3.266 g/cm^3
Absorption coefficient	18.799 mm^{-1}
F(000)	3404
Theta range for data collection	2.36 to 27.49°
Index ranges	$-22\leqslant h\leqslant 22$, $-22\leqslant k\leqslant 21$, $-12\leqslant l\leqslant 16$
Reflections collected	12381
Independent reflections	2383 [R(int) = 0.0308]
Max. and min. transmission	0.3140 and 0.0710
Data / restraints / parameters	2383 / 6 / 145
Goodness-of-fit on F^2	1.182
Final R indices $I>2\sigma(I)$	R_1 = 0.0330, wR_2 = 0.1053
Final R indices all data	R_1 = 0.0347, wR_2 = 0.1126
Largest diff. peak and hole	2.61 and -1.51 $eÅ^{-3}$

S5 Crystal structures

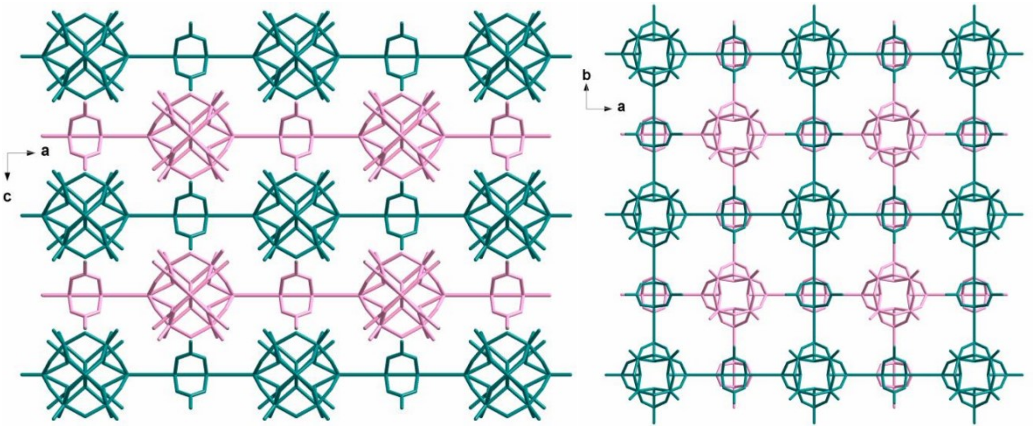

Figure S1. Representation of the AB stacking mode in **1**. The A layer is shown as teal sticks, and the B layer is shown as rose sticks.

S6 Fourier Transform Infrared Spectroscopy (FTIR)

The FT-IR spectrum shows the characteristic peaks in **1**. There is a very obvious and apparent signals stretching between 500 and 900 cm^{-1}. Tungstate POMs characteristically exhibit this signal as it corresponds to the W-O-W bridges generally present in the structures. Also of note is the very sharp peak at 933.2 cm^{-1}. This is also characteristic of tungstate POM, corresponding to the double bond between the tungsten atom and the terminal oxo-ligands. In addition to these characteristic stretching frequencies common to many POMs, it is difficult to meaningfully assign specific signals to specific parts of the structure because the highly connected nature of these molecules changes the degrees of freedom available for individual atoms and groups. However, there is one more signal that could feasibly be assigned. Broad peaks around 3450 cm^{-1} is characteristic of the O-H bonds in the hydroxyl groups of the water molecules.

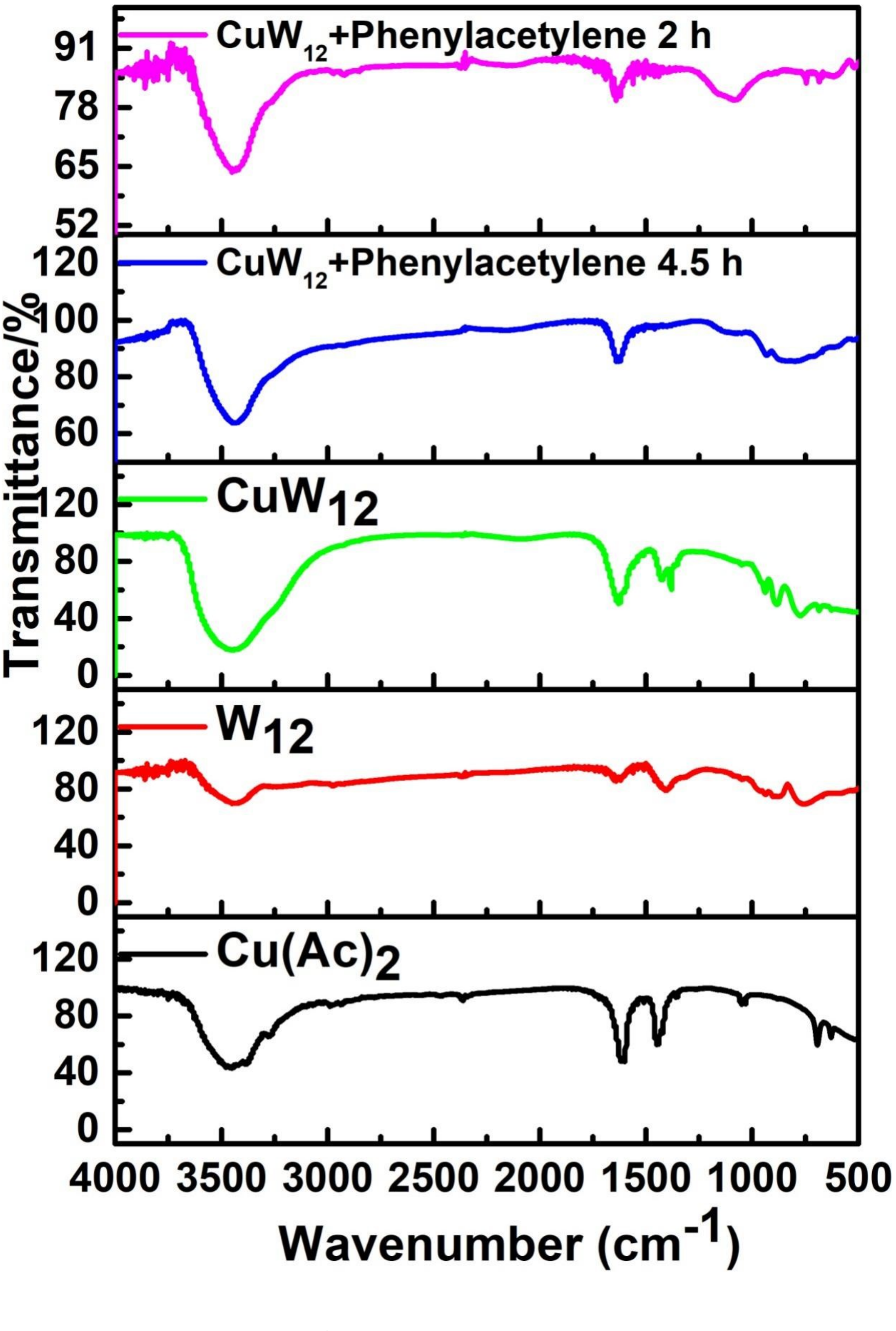

Figure S2 FT-IR spectra of **1**.

S7 Powder X-ray diffraction (PXRD)

The Powder X-ray diffraction (PXRD) patterns for **1** can be compared with the simulated pattern obtained from the X-ray single-crystal diffraction analysis. Their peak positions are in good agreement with each other, indicating the phase purity of the product. The differences in intensity may be due to the preferred orientation of the powder sample.

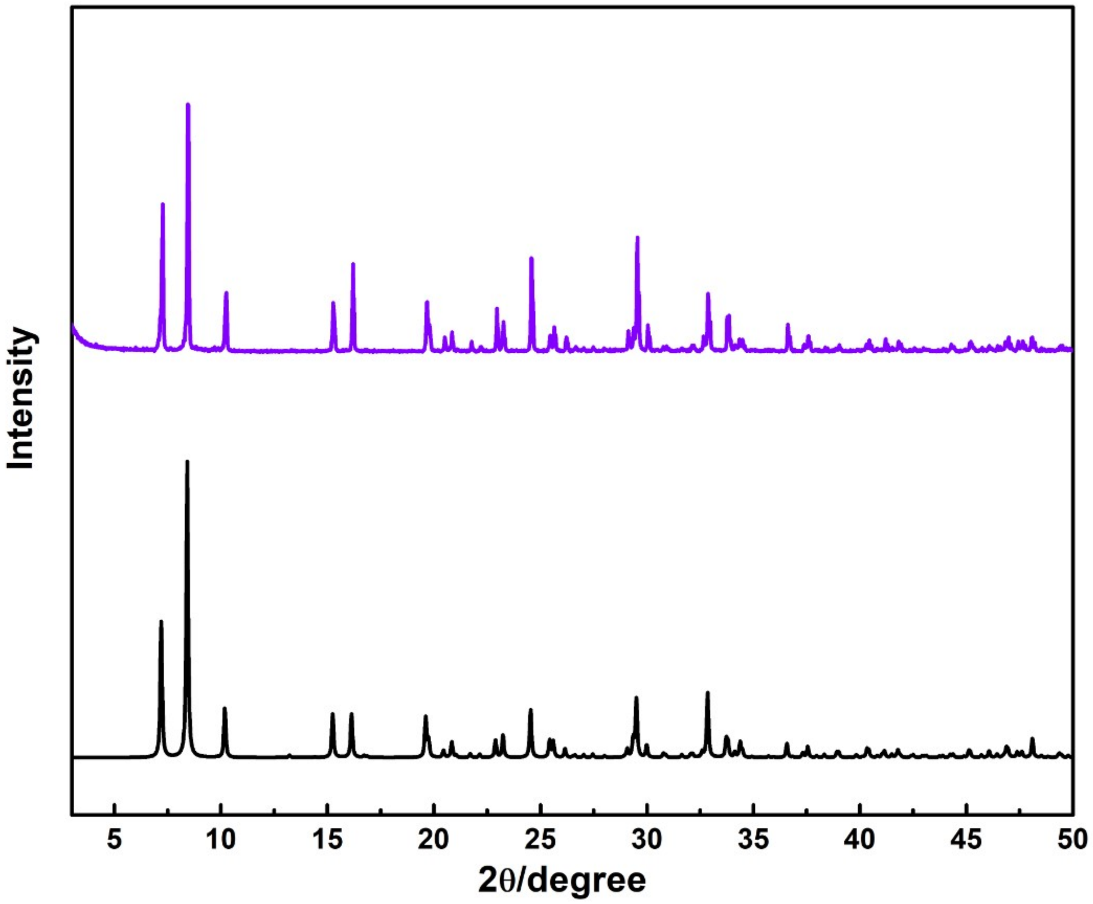

Figure S3 Experimental (purple, **1**) and simulated (black) PXRD patterns.

S8 Thermogravimetric analyses (TGA)

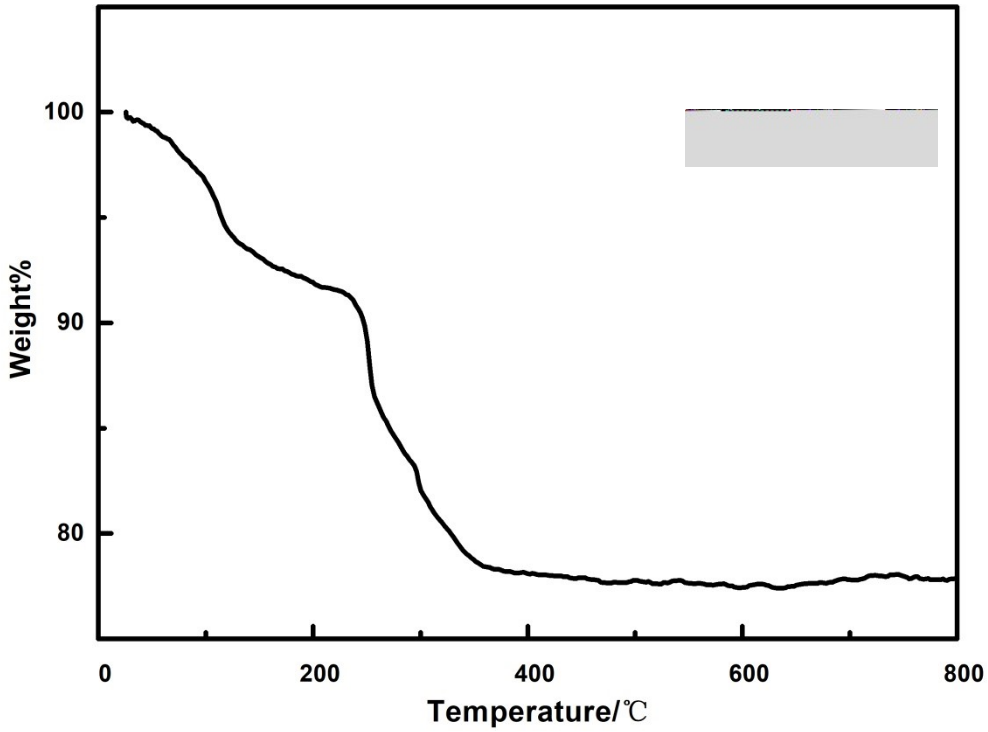

Figure S4 TGA curves of **1**. TGA of **1** shows a weight loss of 6.8 % corresponding to the 15 free water in **1**.

S9 Gas chromatography of catalytic test (Table 1)

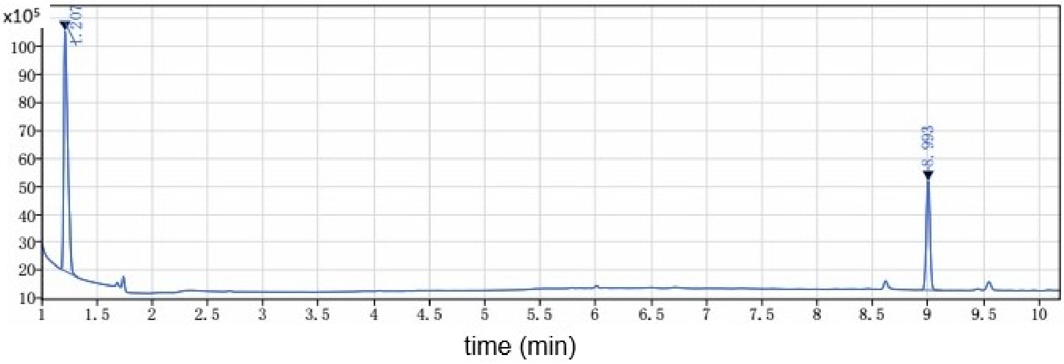

1	signal	FIFIA			
retention time（t）	Type	peak width	peak area	height	（peak area）%
1.207	BB	0.15	219.17	85.80	71.23
8.993	BB	0.19	88.52	39.01	28.77

Figure S5 gas chromatography of Entry 1

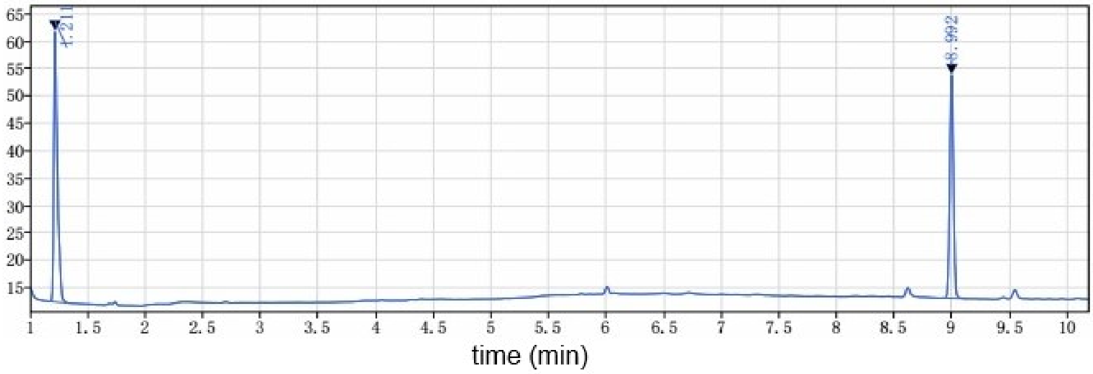

2	signal	FIFIA			
retention time（t）	Type	peak width	peak area	height	（peak area）%
1.211	BB	0.18	109.08	49.46	54.57
8.992	BB	0.19	90.80	40.86	45.43

Figure S6 gas chromatography of Entry 2

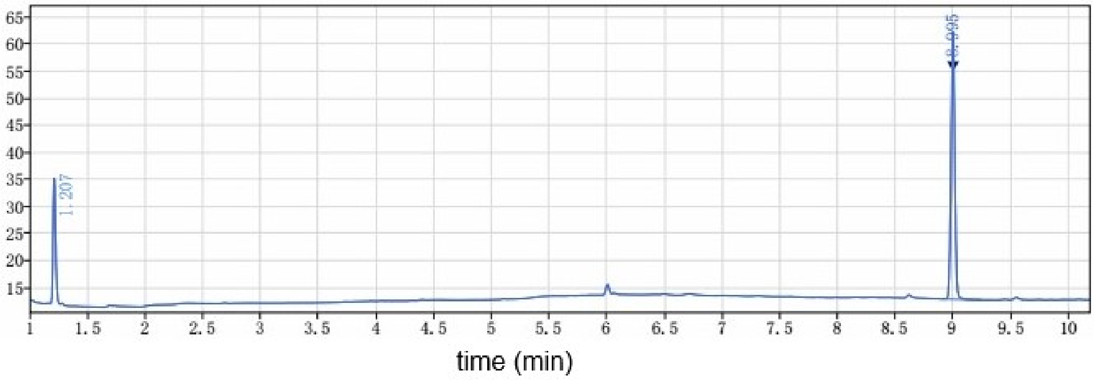

3	signal	FIFIA			
retention time（t）	Type	peak width	peak area	height	（peak area）%
1.207	BB	0.08	34.43	23.09	23.55
8.995	BB	0.32	111.75	49.52	76.45

Figure S7 gas chromatography of Entry 3

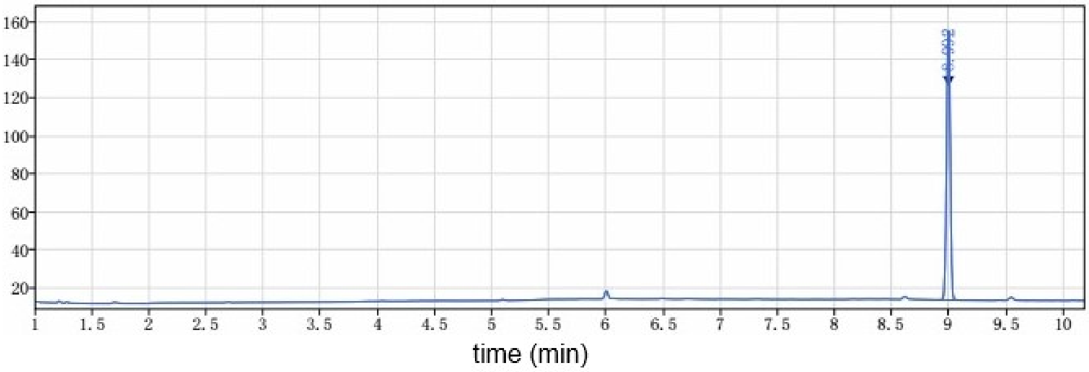

4	signal	FIFIA			
retention time（t）	Type	peak width	peak area	height	（peak area）%
8.992	BB	0.23	313.53	112.01	100

Figure S8 gas chromatography of Entry 4

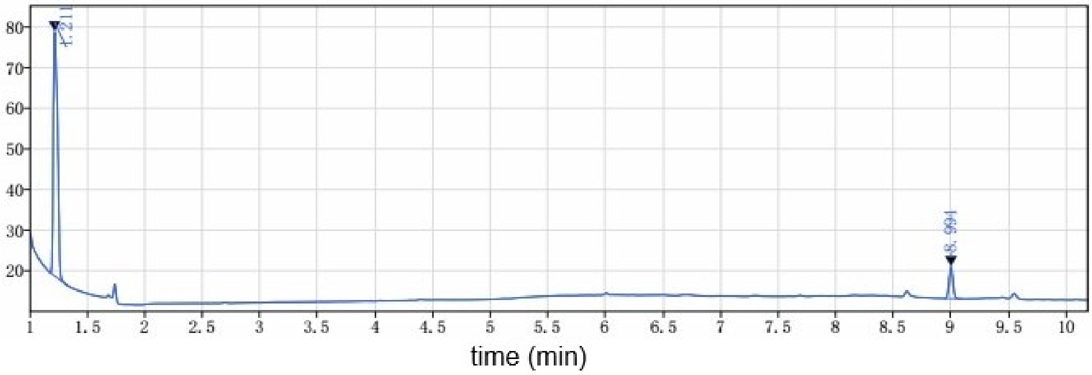

5	signal	FIFIA			
retention time（t）	Type	peak width	peak area	height	（peak area）%
1.211	BV	0.15	150.46	60.24	89.36
8.994	BB	0.17	17.91	7.85	10.64

Figure S9 gas chromatography of Entry 5

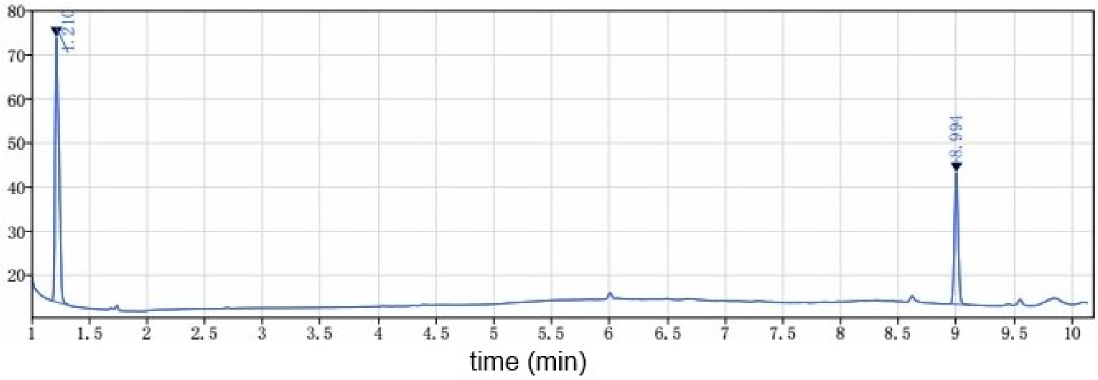

6	signal	FIFIA			
retention time（t）	Type	peak width	peak area	height	（peak area）%
1.210	BV	0.16	137.78	60.12	67.11
8.994	BB	0.19	67.51	21.86	32.89

Figure S10 gas chromatography of Entry 6

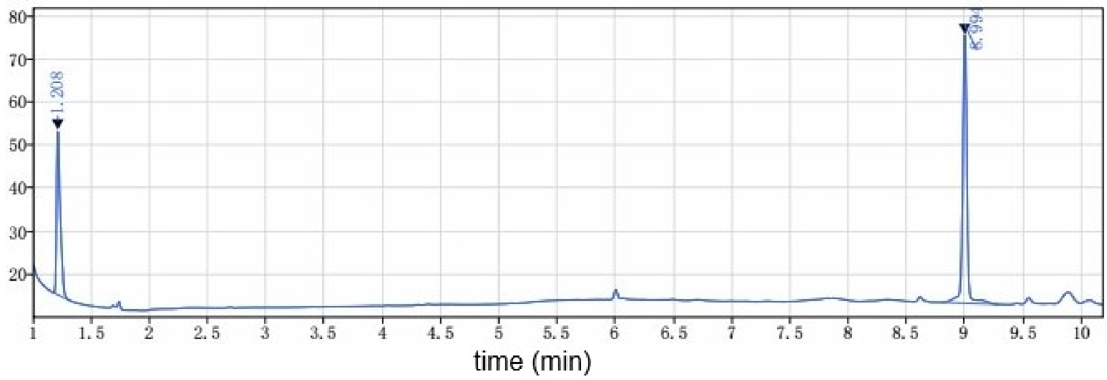

7	signal	FIFIA			
retention time（t）	Type	peak width	peak area	height	（peak area）%
1.208	BB	0.14	83.64	38.30	34.07
8.994	BB	0.49	161.82	62.45	65.93

Figure S11 gas chromatography of Entry 7

8	signal	FIFIA			
retention time（t）	Type	peak width	peak area	height	（peak area）%
8.992	BB	0.19	93.41	41.87	100

Figure S12 gas chromatography of Entry 8

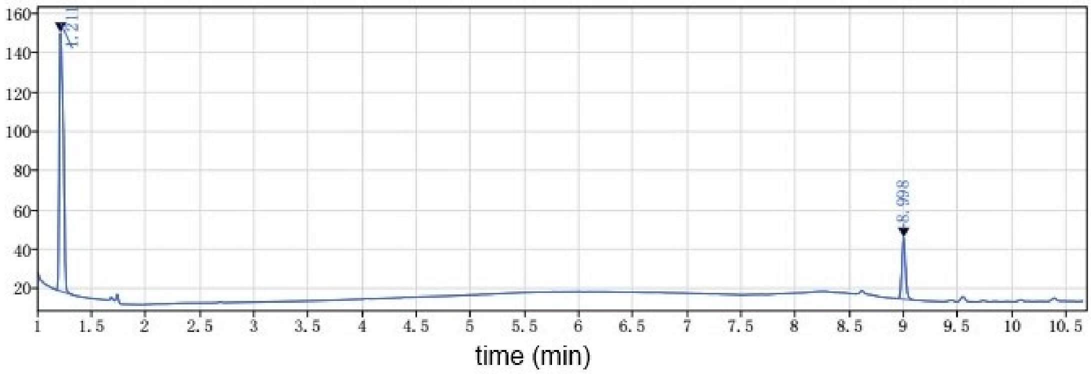

9	signal	FIFIA			
retention time（t）	Type	peak width	peak area	height	（peak area）%
1.211	BB	0.15	329.72	131.62	81.38
8.998	BB	0.16	75.44	31.17	18.62

Figure S13 gas chromatography of Entry 9

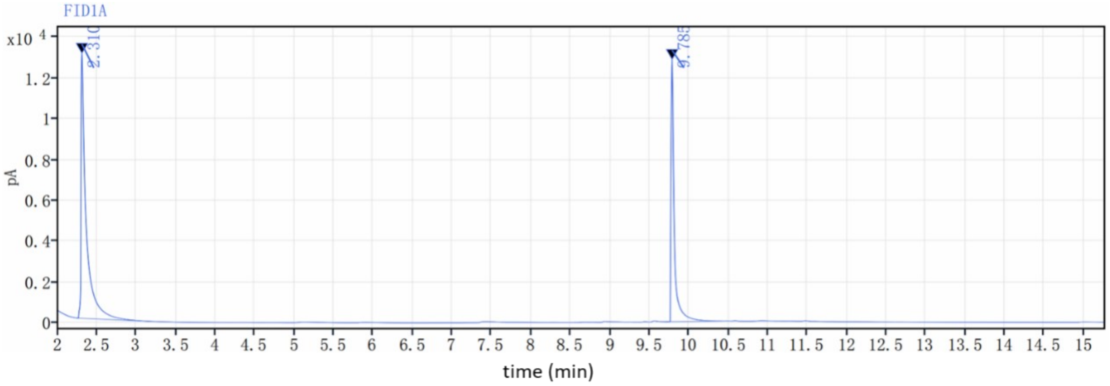

11	signal	FIFIA			
retention time（t）	Type	peak width	peak area	height	（peak area）%
2.310	BB	0.92	58814.59	12937.75	61.46
9.785	BB	0.74	36878.78	12804.77	38.54

Figure S14 gas chromatography of Entry 11

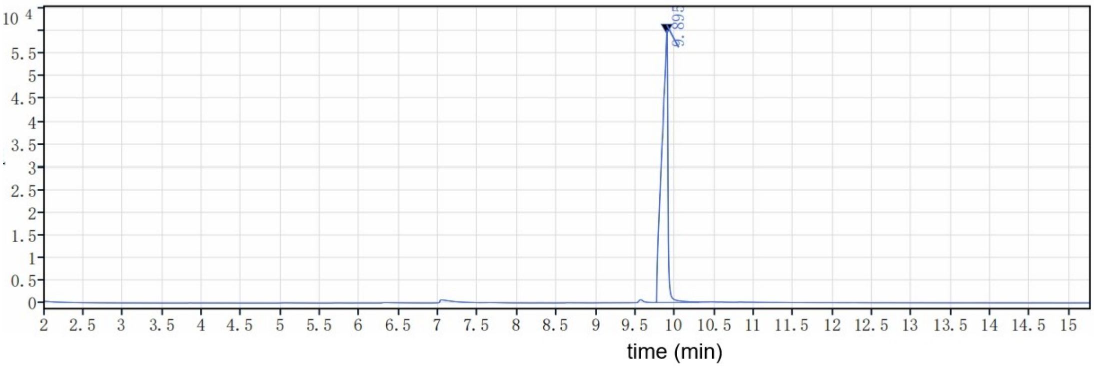

12	signal	FIFIA			
retention time（t）	Type	peak width	peak area	height	（peak area）%
9.895	BV	0.57	319000.18	59126.94	100

Figure S15 gas chromatography of Entry 12

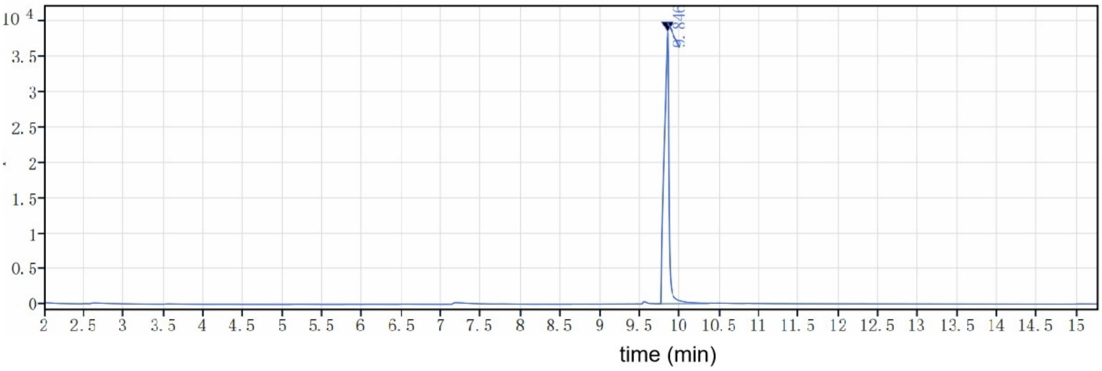

13	signal	FIFIA			
retention time（t）	Type	peak width	peak area	height	（peak area）%
9.846	BV	0.63	152488.51	38411.15	100

Figure S16 gas chromatography of Entry 13

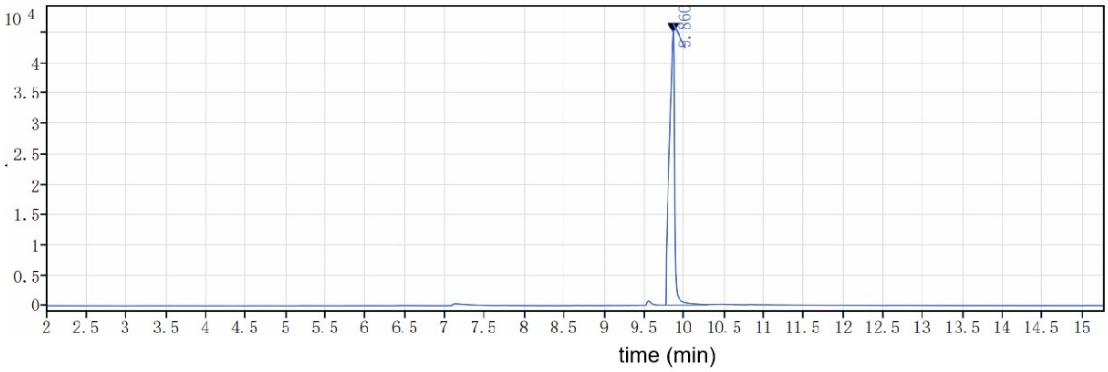

14	signal	FIFIA			
retention time（t）	Type	peak width	peak area	height	（peak area）%
9.860	BV	0.56	205777.65	44805.94	100

Figure S17 gas chromatography of Entry 14

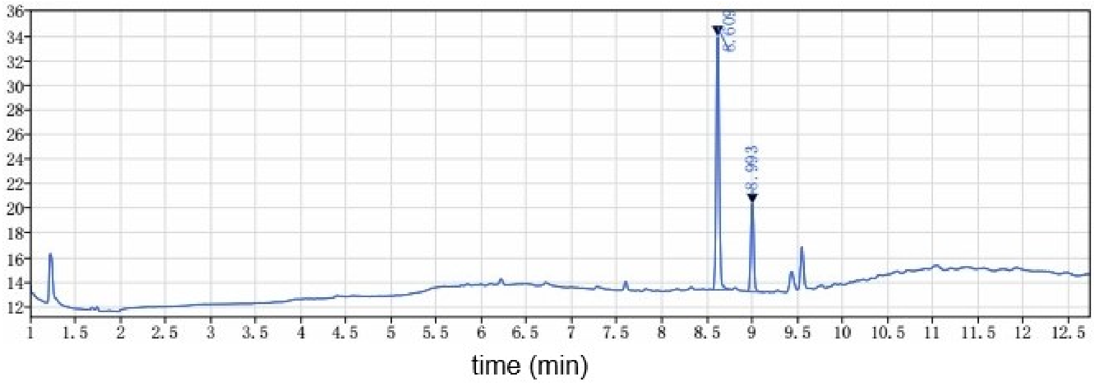

15	signal	FIFIA			
retention time（t）	Type	peak width	peak area	height	（peak area）%
8.609	BB	0.21	47.63	20.56	74.47
8.993	BB	0.18	16.33	7.11	25.53

Figure S18 gas chromatography of Entry 15

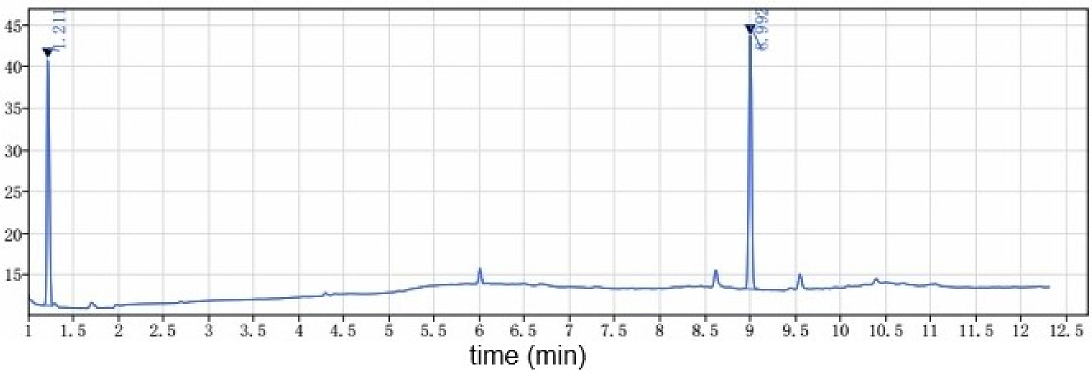

16	signal	FIFIA			
retention time（t）	Type	peak width	peak area	height	（peak area）%
1.211	BB	0.10	56.89	29.57	45.18
8.992	BB	0.20	69.02	30.40	54.82

Figure S19 gas chromatography of Entry 16

S10 Gas chromatography of catalytic test (Table 2)

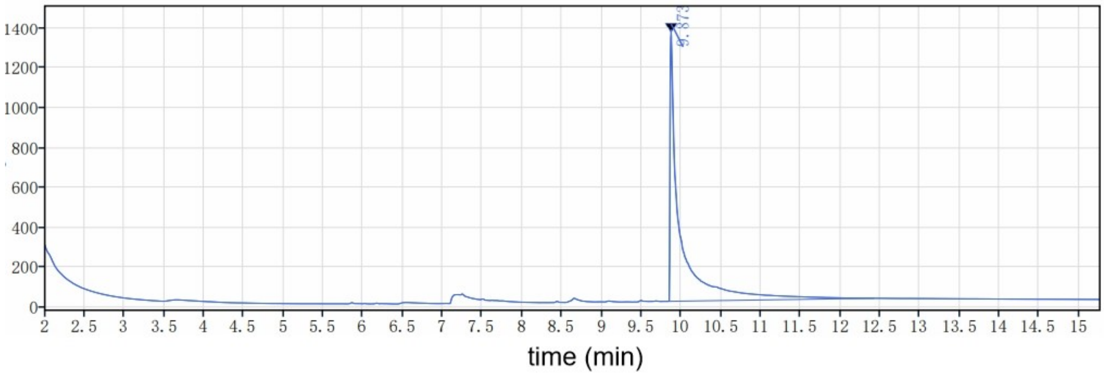

1	signal	FIFIA			
retention time（t）	Type	peak width	peak area	height	（peak area）%
9.873	BB	2.61	11695.05	1344.01	100

Figure S20 gas chromatography of Entry 1

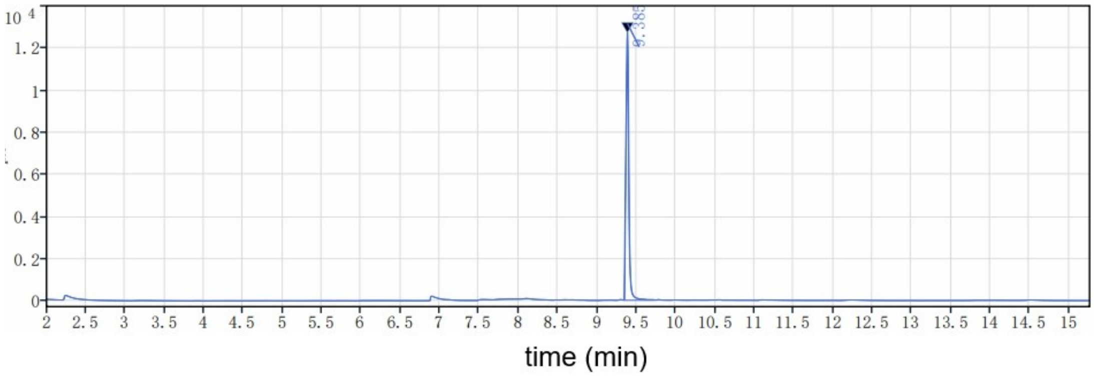

2	signal	FIFIA			
retention time（t）	Type	peak width	peak area	height	（peak area）%
9.385	VV	0.41	32374.54	12675.20	100

Figure S21 gas chromatography of Entry 2

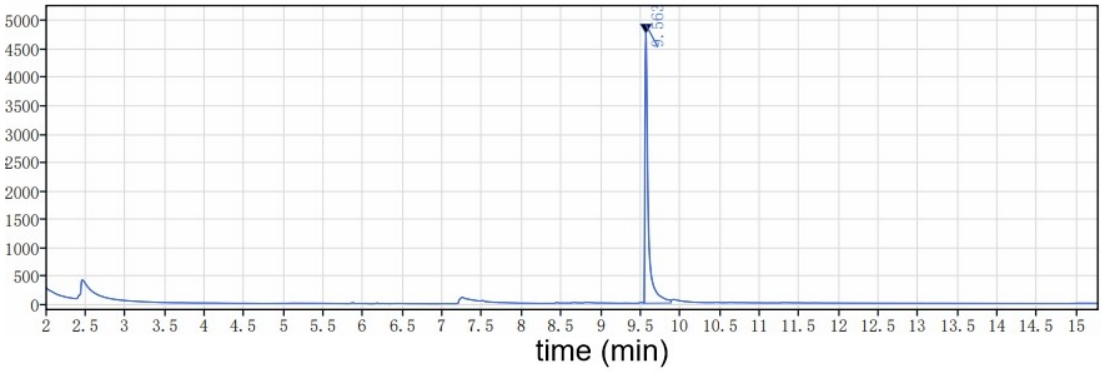

3	signal	FIFIA			
retention time（t）	Type	peak width	peak area	height	（peak area）%
9.563	VV	0.35	13569.80	4740.75	100

Figure S22 gas chromatography of Entry 3

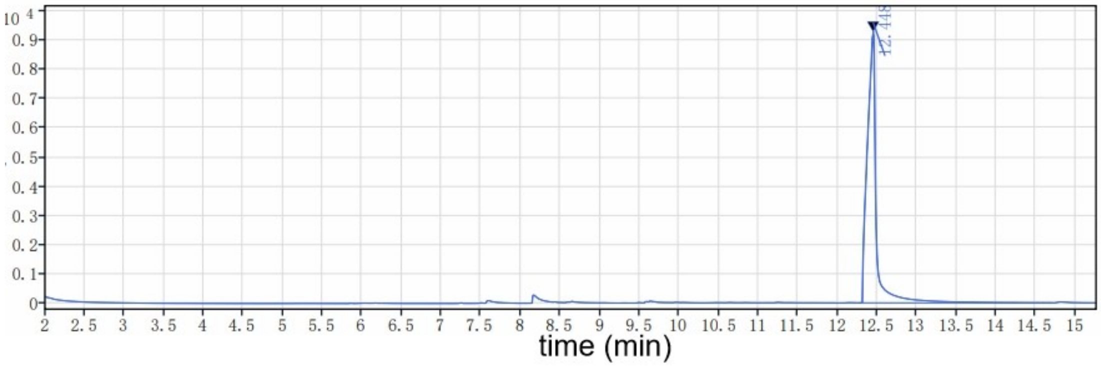

4	signal	FIFIA			
retention time（t）	Type	peak width	peak area	height	（peak area）%
12.448	BB	2.43	72694.25	9236.84	100

Figure S23 gas chromatography of Entry 4

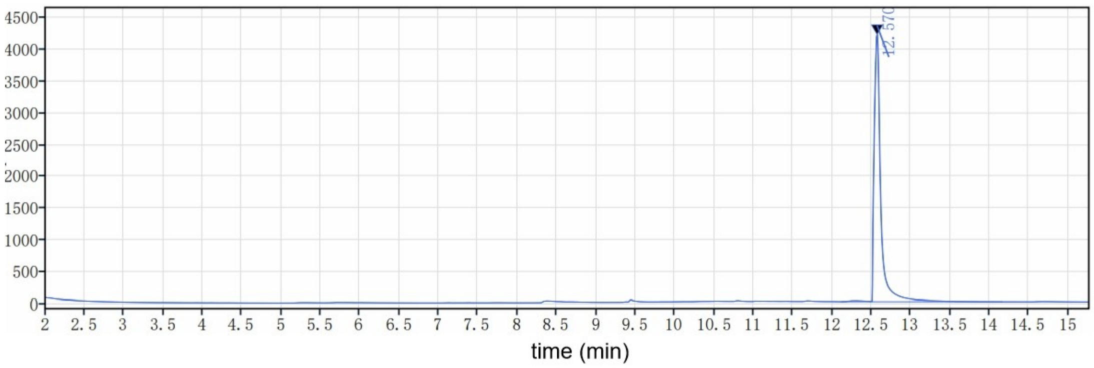

5	signal	FIFIA			
retention time（t）	Type	peak width	peak area	height	（peak area）%
12.570	BBA	1.89	24676.55	4200.89	100

Figure S24 gas chromatography of Entry 5

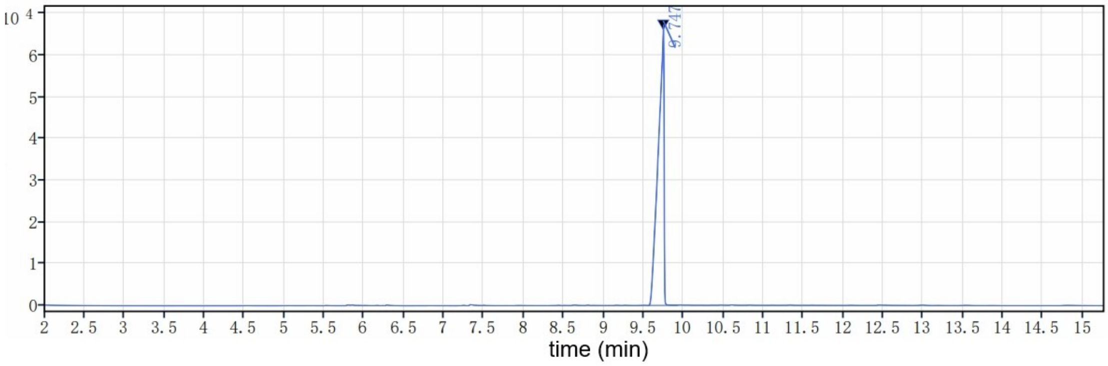

7	signal	FIFIA			
retention time（t）	Type	peak width	peak area	height	（peak area）%
9.747	BV	0.37	340188.46	65807.93	100

Figure S25 gas chromatography of Entry 6

S11 Gas chromatography mass spectrometry

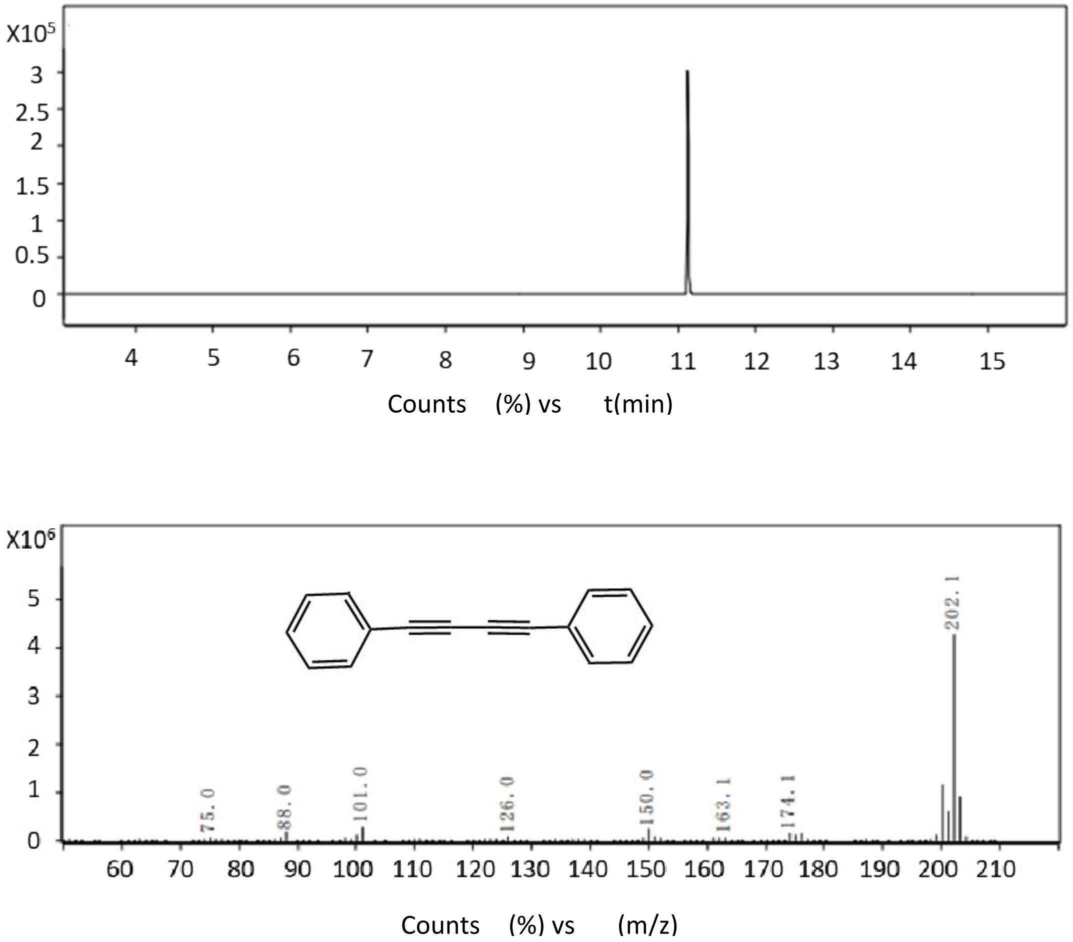

Figure S26 Gas chromatography mass spectrometer for catalytic test of coupling products

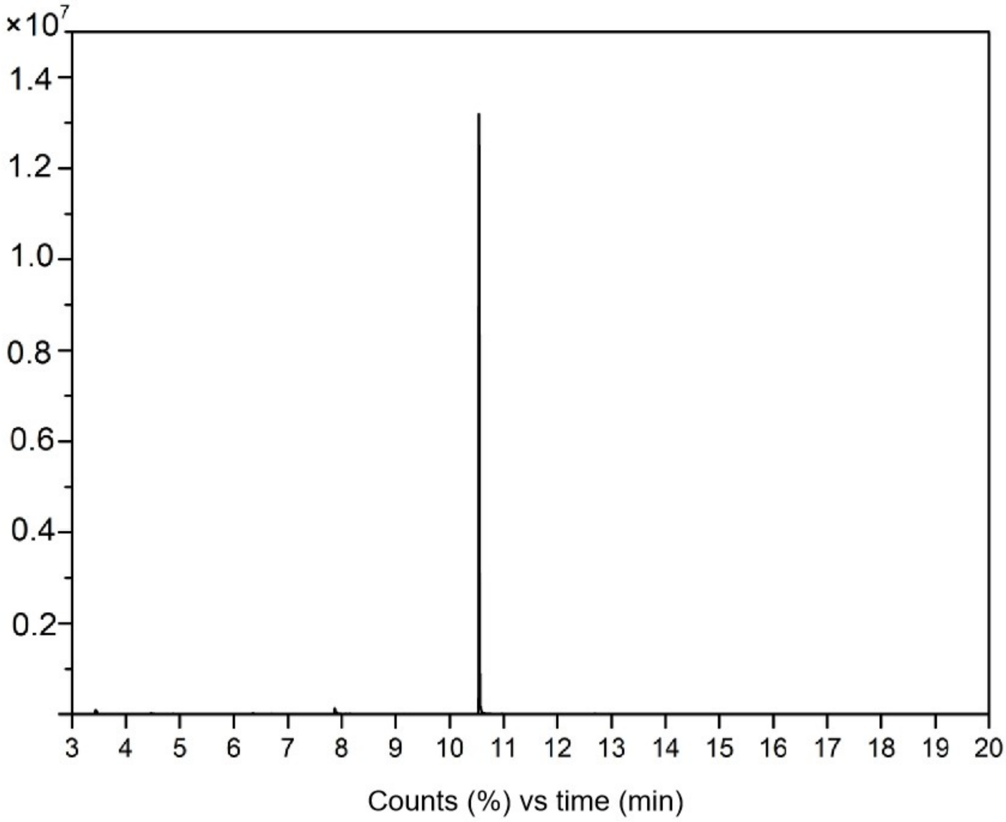

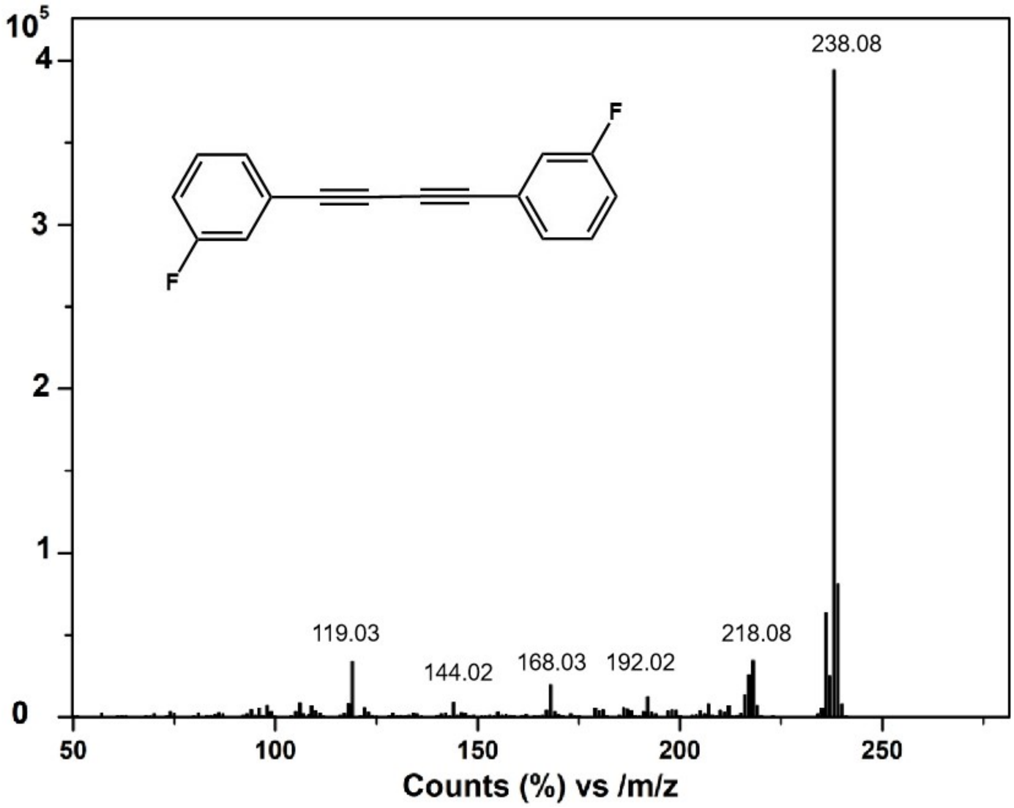

Figure S27 Gas chromatography mass spectrometer for catalytic test of coupling products

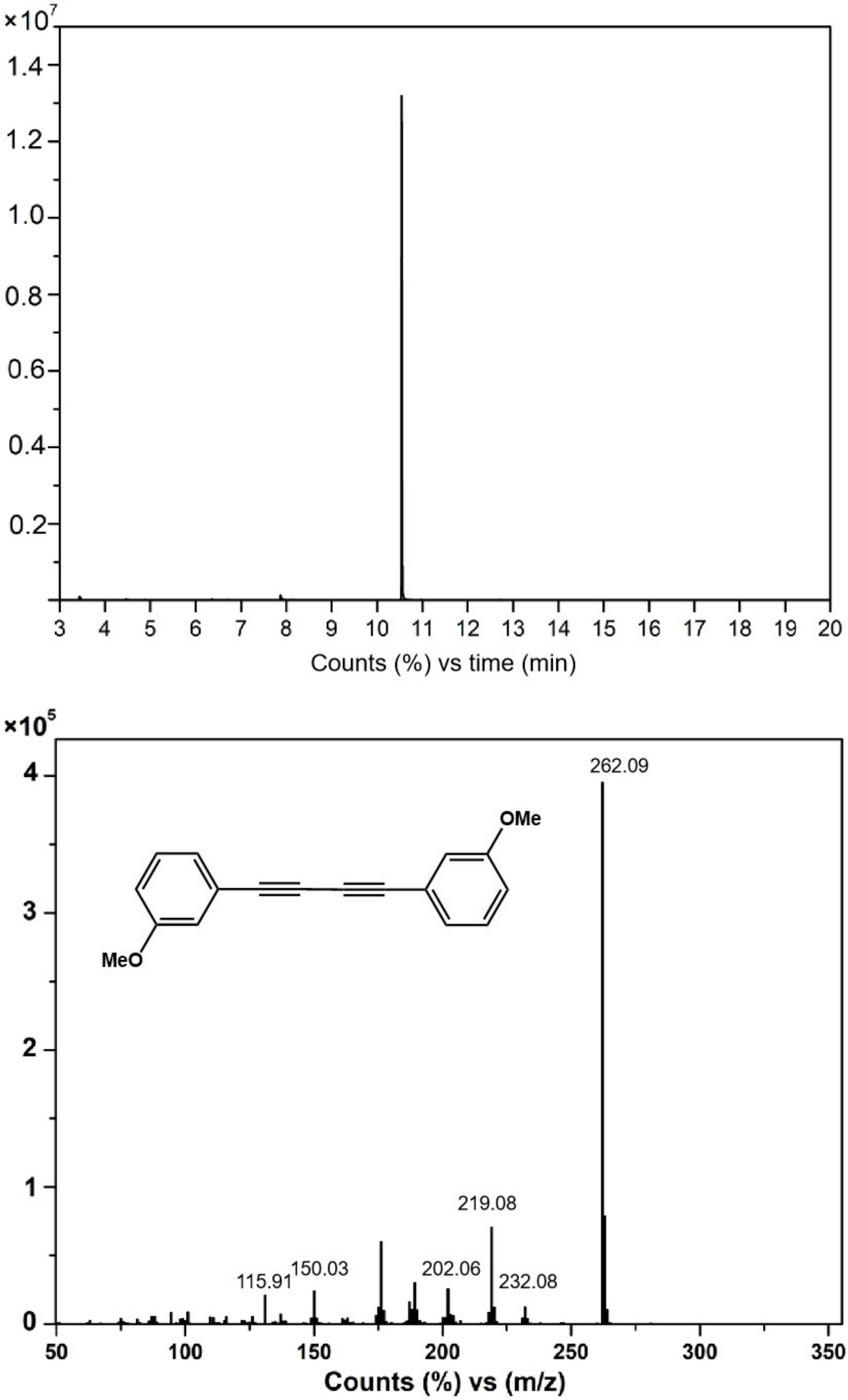

Figure S28 Gas chromatography mass spectrometer for catalytic test of coupling products

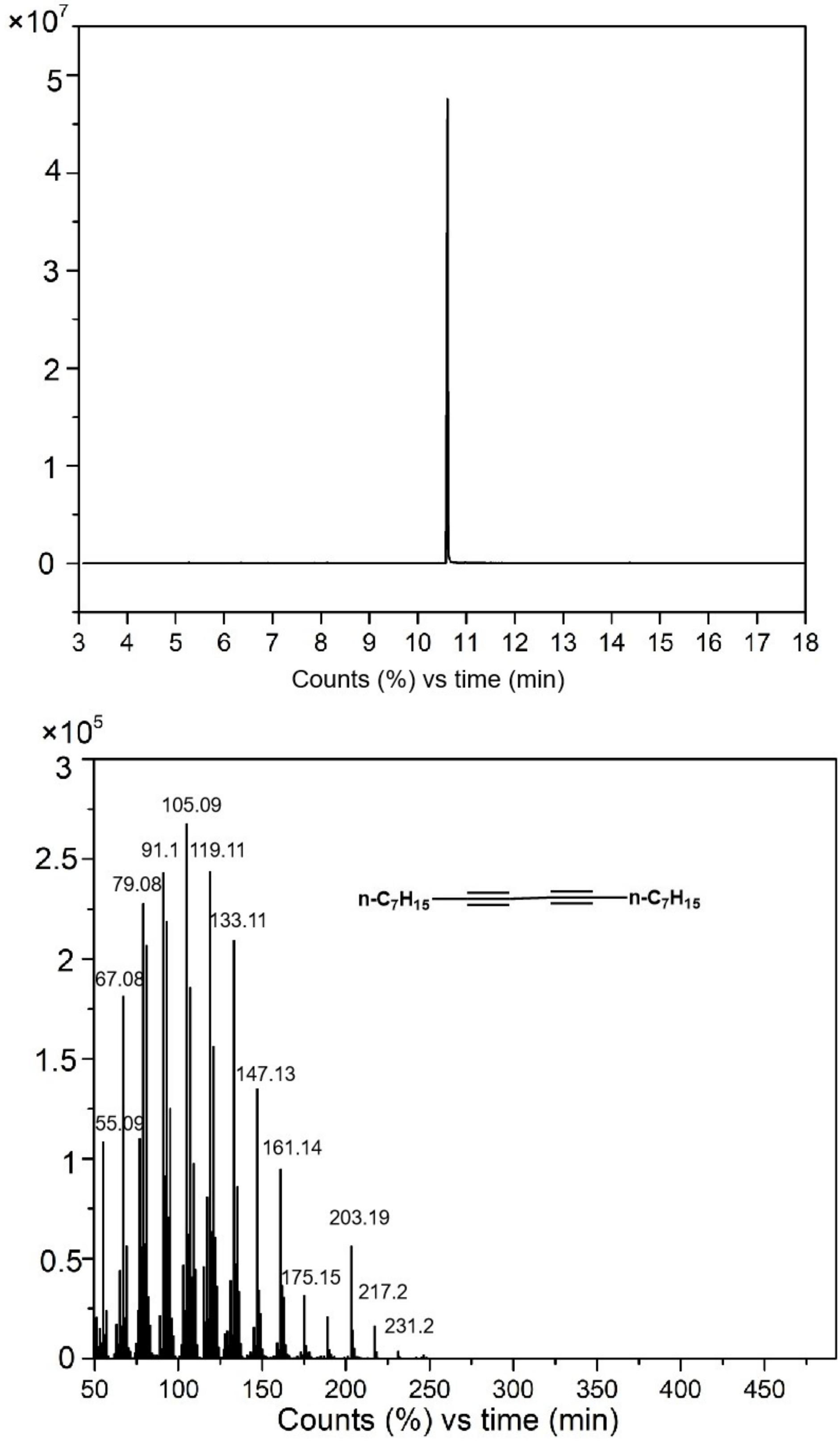

Figure S29 Gas chromatography mass spectrometer for catalytic test of coupling products

S12. ESI-MS

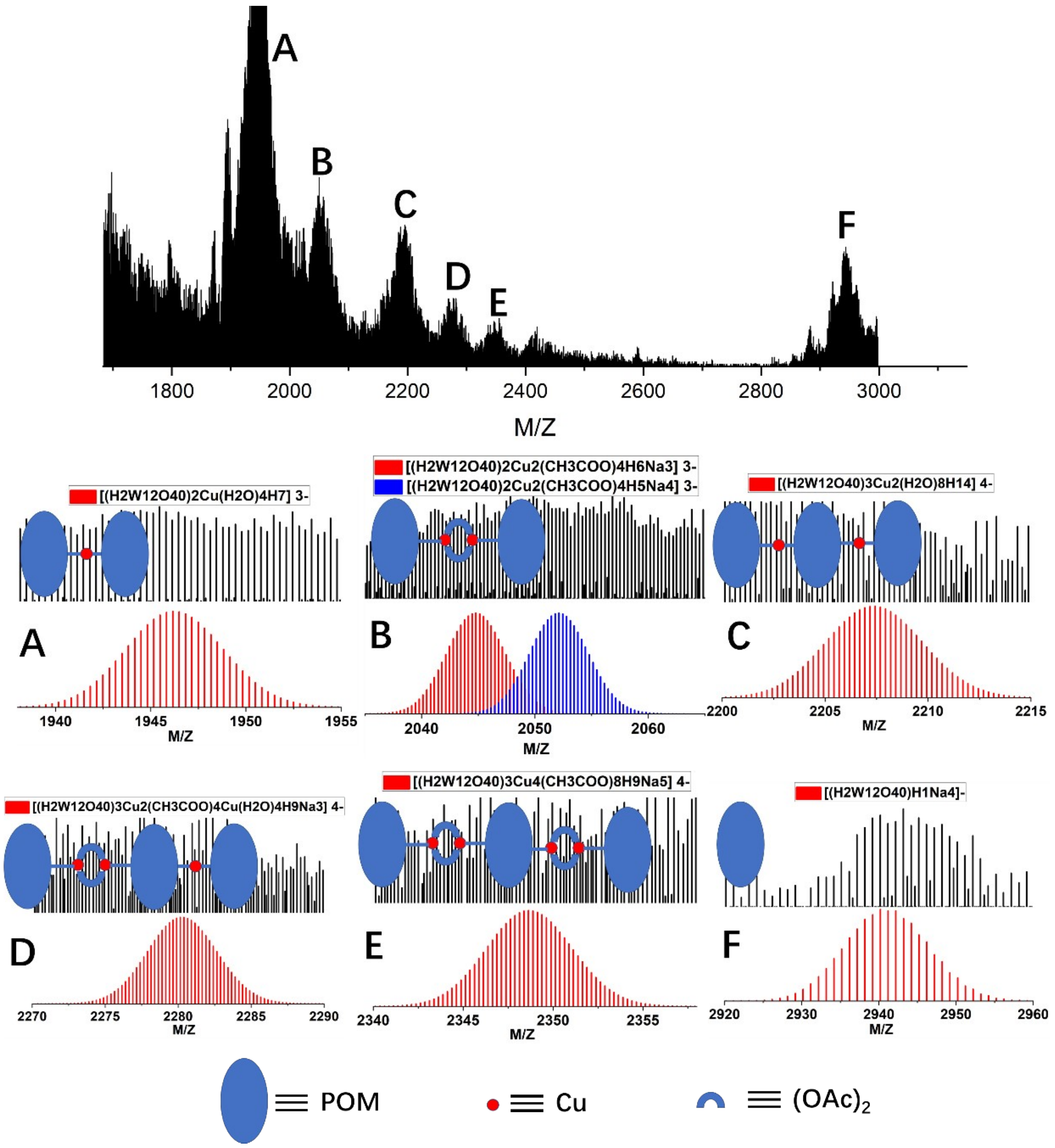

Figure S30. ESI mass spectrum of the catalyst after catalytic reaction.

S13. DFT calculation

Calculations were performed by using the Perdew, Burke, Ernzerhof (PBE) functional of generalized gradient approximation (GGA as implemented in Vienna ab-initio Simulation Package (VASP). The cutoff energy is 450 eV was applied to describe the valence electron density. The convergence threshold was 10^{-5} eV in energy and 10^{-2} eV/Å in force. The Brillouin zone was sampled as 1∅1∅1.We only considered the dimer units containing W, Cu, O, H and F atoms which are shown in the Figure S32 (up panel).

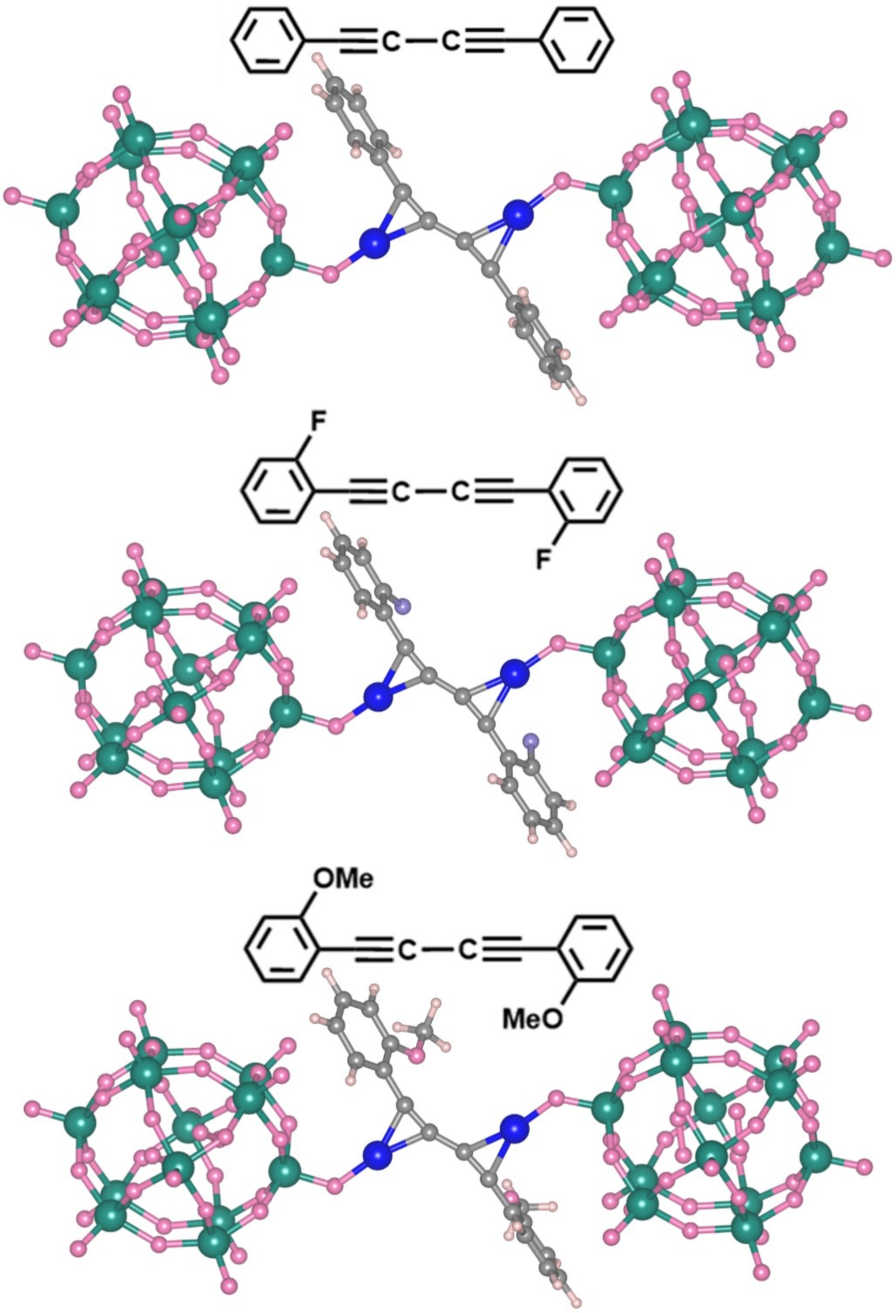

Figure S31. Model structure of alkynes on {POM_2-Cu_2}.

The two peaks of gas chromatograms belong to substrates (Acetylene) and coupling products, separately. (Entry 1-14, DMF as solvent). The products were verified by standard samples or gas chromatography-mass spectrometer. When THF as solvent (Entry 15, 16), the catalyst is largely decomposed after reaction as shown in Figure S33, the baseline of chromatograms becomes quite noisy and other peaks appear.

Figure S32. Photos of supernatant of Entry 15 and 16. The deionized water was firstly added to the reaction mixture and then extracted with diethyl ether to get the supernatant.

Table S2. Yield of POM-based catalysts, copper-dimer-based catalysts Reported in the Literature and Present Work for Phenylacetylene.

Catalyst	Yield (%)	Additive(base)	Oxidant	Substrate/Catalyst Ratio	Temp. (K)	Time (h)	Refs
CuI	99	K_2CO_3	-	50/1	393	12h	2
$Cu(OTf)_2$	92	DBU(1,8-Diazabicyclo [5.4.0]undec-7-ene)	O_2	20/1	r.t.	2-5h	3
Cu NPs-OMCN	98	-	O_2	1/1	333	24h	4
Cu-Pol	98	Pyridine	air	200/1	r.t.	14h	5
Cu^I/SiO_2	96	Piperidine	air	50/1	373	3h	6
Cu/C_3N_4	99	IPA(iso-propyl alcohol)	O_2	5/1	r.t.	12h	7
$SiW_{10}Cu_2$	93	-	O_2	500/1	373	18h	8
1	>99	-	-	33/1	363	3.5h	This work

S14 Reference

1 Sheldrick, G. M. *Acta Cryst. A* **2008**, 64, 112.

2. SINGH M, SINGH A S, MISHRA N, et al. Benzotriazole as an Efficient Ligand in Cu-Catalyzed Glaser Reaction [J]. ACS Omega, 2019, 4(1): 2418-2424.

3. HOLGANZA M K, TRIGOURA L, ELFARRA S, et al. Copper (II) catalyzed homocoupling and heterocoupling of terminal alkynes [J]. Tetrahedron Letters, 2019, 60(17): 1179-1181.

4. XU H, WU L, TIAN J, et al. Copper Nanoparticles on Ordered Mesoporous Carbon Nitride Support: a Superior Catalyst for Homo- and Cross-Coupling of Terminal Alkynes under Base-Free Conditions [J]. European Journal of Organic Chemistry, 2019(39): 6690-6696.

5. ZURAEV A V, GRIGORIEV Y V, IVASHKEVICH L S, et al. Copper-Polymer Nanocomposite Catalyst for Synthesis of 1,4-Diphenylbutadiyne-1,3 [J]. Zeitschrift für anorganische und allgemeine Chemie, 2017, 643(19): 1215-1219.

6. VAN GELDEREN L, ROTHENBERG G, ROBERTO CALDERONE V, et al. Efficient alkyne homocoupling catalysed by copper immobilized on functionalized silica [J]. Applied Organometallic Chemistry, 2013, 27(1): 23-27.

7. XU H, WU K, TIAN J, et al. Recyclable Cu/C3N4 composite catalysed homo- and cross-coupling of terminal alkynes under mild conditions [J]. Green Chemistry, 2018, 20(4): 793-797.

8.Kamata K, Yamaguchi S, Kotani M, et al., Efficient oxidative alkyne homocoupling catalyzed by a monomeric dicopper-substituted silicotungstate[J]. Angew Chem Int Ed Engl, 2008, 47(13), 2407-2410.